SCIENCE CHINA
Information Sciences

• **Supplementary File** •

Precoder and Combiner Design for Dynamically Sub-Connected Hybrid Architecture with Low-Resolution DACs/ADCs in mmWave Massive MIMO Systems

Xiaorong JING[1,2,3*], Lianghong LI[1], Hongqing LIU[1,2,3] & Qianbin CHEN[1,2,3]

[1]*School of Communication and Information Engineering, Chongqing University of Posts and Telecommunications, Chongqing* 400065*, China;*
[2]*Chongqing Key Laboratory of Mobile Communications Technology, Chongqing* 400065*, China;*
[3]*Engineering Research Center of Mobile Communications, Ministry of Education, Chongqing* 400065*, China*

Appendix A Related work

Appendix A.1 Precoder and/or Combiner Design for HA with Full Precision DACs/ADCs

The existing HAs with full precision DACs/ADCs are mainly classified as fully-connected hybrid architecture (FC-HA) and sub-connected hybrid architecture (SC-HA) in terms of the connection mode between RF chain and the transmit antennas. For FC-HA, each RF chain is connected to all the transmit antennas, while for SC-HA, each RF is connected to a disjoint subset of the total transmit antennas. In the case of FC-HA, the authors in [1] proposed an orthogonal matching pursuit (OMP)-based precoder and combiner design scheme. By conditionally maximizing the spectral efficiency, the authors in [2] proposed an iterative algorithm to design the analog precoder and combiner with low resolution. Li J et al proposed an energy-efficient HA to design the analogy and digital beamformers [3], in which the Butler phase shifting matrix was utilized to overcome the drawbacks of the conventional phase shifters. In [4], the authors proposed a hybrid precoder based on joint iterative training with low-resolution phase shifters (PSs) for downlink communications to avoid the high-dimensional channel estimation. Despite the good performance of these FC-HAs, the number of APSs required is as large as the product of the number of the transmit antennas and the number of RF chains. Moreover, RF adders required are equal to the number of the transmit antennas. All these mean high power consumption and hardware cost for FC-HAs.

Compared with FC-HA, SC-HA, where RF chains are exclusively connected to the corresponding transmit antenna subsets, greatly reduces the number of APSs required. Thus, by introducing an adaptive connection mode between RF chains and APSs, an adaptive hybrid precoder was proposed in [5]. Compared with the typical FSC-HA, in which each RF is connected to the fixed disjoint subset of the total transmit antennas [6], the adaptive hybrid precoder achieved certain performance advantages, but it is not flexible enough without considering the differences of each channel between the transmit antennas to different users. Between RF chains and APSs, a dynamic connection network was inserted to form the DSC-HA, in which each RF is connected to a disjoint subset (with non-fixed number) of total transmit antennas, and the transmit antennas connected to each RF vary with the channel conditions [7]. DSC-HA achieved a better performance than FSC-HA, and it also has obvious advantages over FD-A and FC-HA in the power consumption and hardware cost. But in DSC-HA, each user is equipped with a single antenna. To take full advantage of the diversity and multiplexing gains provided by MIMO technology, the user terminal is desired to be configured with multiple antenna, which complicates the precoder and combiner design for DSC-HA. Meanwhile, DACs/ADCs are assumed to be with ideal resolution as FC-HA. The authors in [8] pointed out that DACs/ADCs' power consumption increases exponentially with resolution and linearly with bandwidth. Since much wider occupied bandwidths at very high frequencies are available in mmWave communications, the huge complexity of the required hardware circuits and power consumption of high-resolution DACs/ADCs prevents one from implementing DSC-HA in practical applications.

Appendix A.2 Precoder and/or Combiner Design for HA with Low-resolution ADCs

From above, the high power consumption and hardware cost of DACs/ADCs becomes a challenge for the implementation of the practical mmWave mMIMO sytems. To alleviate this predicament, the hybrid precoder with low-resolution ADCs have gained increasing interests recently. In [9], the authors discussed several important issues with low-resolution ADCs, including transmit precoding, on mmWave mMIMO systems. Under AQNM, the energy and spectral efficiency of digital and hybrid beamformers were compared in the case of low resolution quantization in [10], where FSC-HA was adopted and led to a much poorer performance than FC-HA. The tradeoff between the power consumption and achievable rate was discussed in HA with a small number of RF chains and limited-resolution ADCs in [11]. In [12], the tradeoff between the energy efficiency and spectral efficiency was investigated for the analog, digital, and hybrid combining schemes with low-resolution ADCs. However, in these schemes, BS was assumed with FD-A, which is obviously not in line with the actual design. For mMIMO systems with hybrid precoding, the authors in [13] proposed an efficient analog combiner design scheme by maximizing an unconstrained mutual information with low-resolution ADCs. However, in these forementioned contributions, ADCs with low resolution, i.e., 1-8 (bits), were considered at the receiver, while the transmitter adopted FD-A or HA with high-resolution DACs.

* Corresponding author (email: jingxr@cqupt.edu.cn)

Appendix A.3 Precoder and/or Combiner Design for HA with Low-resolution DACs

Besides many works of the precoder and/or combiner design for HA with low-resolution ADCs only, a few closely related studies of application of low-resolution DACs, i.e., 1-8 (bits), at the transmitter have emerged. Based on the AQNM, the work in [14] performed the hybrid precoder design for FC-HA and SC-HA with low-resolution DACs, where APSs with low resolution were utilized to realize the analog precoder. For mmWave MIMO systems, an energy-efficient hybrid precoder with low-resolution DACs was designed in [15].

Appendix B System description

Appendix B.1 Signal model

With the system configuration in Fig.1 and after hybrid precoding, the transmitted signal from the BS is written as [14]

$$\mathbf{x} = \mathbf{F}_{\mathrm{RF}} Q_B(\mathbf{F}_{\mathrm{BB}}\mathbf{s}), \tag{B1}$$

where $Q_B(\cdot)$ denotes the vector quantizer with B bits, $\mathbf{s} = [s_1, s_2, \cdots, s_K]^T \in \mathbb{C}^{K\times 1}$ satisfying with $\mathbb{E}\left\{\mathbf{s}\mathbf{s}^H\right\} = \frac{P}{K}\mathbf{I}_K$ with P denoting the total transmitting power of the BS antennas, $\mathbf{F}_{\mathrm{RF}} = \left[\mathbf{f}_{\mathrm{RF}}^1, \mathbf{f}_{\mathrm{RF}}^2, \cdots, \mathbf{f}_{\mathrm{RF}}^K\right] \in \mathbb{C}^{M\times K}$ is the analog precoder, and $|\mathbf{F}_{\mathrm{RF}}(m,k)| = \frac{1}{\sqrt{N_{\mathrm{sub}}^k}}$ for $\mathbf{F}_{\mathrm{RF}}(m,k) \neq 0$ with $\mathbf{F}_{\mathrm{RF}}(m,k)$ and N_{sub}^k denoting the (m,k)th element of $\mathbf{F}_{\mathrm{RF}}$ and the number of antennas exclusively connected with the kth transmit RF chain satisfied with $\sum_{k=1}^{K} N_{\mathrm{sub}}^k = M$, receptively, $\mathbf{F}_{\mathrm{BB}} = \left[\mathbf{f}_{\mathrm{BB}}^1, \mathbf{f}_{\mathrm{BB}}^2, \cdots, \mathbf{f}_{\mathrm{BB}}^K\right] \in \mathbb{C}^{K\times K}$ is the digital precoder, while $\mathbf{F}_{\mathrm{RF}}$ and $\mathbf{F}_{\mathrm{BB}}$ are linked through the total power constraints, i.e., $\|\mathbf{F}_{\mathrm{RF}}\mathbf{F}_{\mathrm{BB}}\|_F^2 = K$. Applying the AQNM, which is widely used because it facilitates analysis and provides insights into quantized system [16], to the precoded signal model (B1), and under assumption that all DACs undergo the same distortion as in [14], the transmitted signal from the BS is further expressed as

$$\mathbf{x} = \alpha\mathbf{F}_{\mathrm{RF}}\mathbf{F}_{BB}\mathbf{s} + \mathbf{F}_{\mathrm{RF}}\mathbf{n}_{q_D}, \tag{B2}$$

where $\alpha = 1-\eta$ with η being equal to $\sqrt{3}\pi 2^{-2B-1}$ for the resolution of the ADC $B > 5$, and the exact values of which is given for $B \leqslant 5$ in [17], and $\mathbf{n}_{q_D}$ denotes the quantization noise vector with variance matrix $\mathbf{R}_{\mathbf{n}_{q_D}}$=Diag$(\sigma^2_{\mathbf{n}_{q_D},1}, \sigma^2_{\mathbf{n}_{q_D},2}, \cdots, \sigma^2_{\mathbf{n}_{q_D},K}) = \frac{P\sqrt{1-\alpha^2}}{K}$diag$(\mathbf{F}_{BB}\mathbf{F}_{BB}^H)$ with Diag$(\mathbf{a})$ and diag$(\mathbf{A})$ indicating the operations of forming a diagonal matrix by putting vector $\mathbf{a}$ on main diagonal and forming a diagonal matrix by taking the main diagonal elements of $\mathbf{A}$, respectively. From Eq. (B2), applying the AQNM to approximate the non-linear distortion in DACs, the transmitted signal has more complex form.

After analog combining, the received signal of the kth user r_k is

$$r_k = \alpha(\mathbf{w}^k)^H\mathbf{H}_k\mathbf{F}_{\mathrm{RF}}\mathbf{f}_{\mathrm{BB}}^k s_k + \alpha(\mathbf{w}^k)^H\mathbf{H}_k\mathbf{F}_{\mathrm{RF}}\sum_{j\neq k}\mathbf{f}_{\mathrm{BB}}^j s_j + (\mathbf{w}^k)^H\mathbf{H}_k\mathbf{F}_{\mathrm{RF}}\mathbf{n}_{q_D} + (\mathbf{w}^k)^H\mathbf{n}_k, \tag{B3}$$

where $\mathbf{H}_k \in \mathbb{C}^{N\times M}$ denotes the channel matrix between the BS and the kth user, $\mathbf{w}^k \in C^{N\times 1}$ is the kth column of the analog combiner $\mathbf{W} = \left[\mathbf{w}^1, \mathbf{w}^2, \cdots, \mathbf{w}^K\right] \in \mathbb{C}^{N\times K}$, and $\mathbf{n}_k \sim \mathbb{CN}(0, \sigma^2\mathbf{I}_N)$ represents additive white Gaussian noise (AWGN). In (B3), $\alpha(\mathbf{w}^k)^H\mathbf{H}_k\mathbf{F}_{\mathrm{RF}}\sum_{j\neq k}\mathbf{f}_{\mathrm{BB}}^j s_j$ is the interference from other $K-1$ users.

In (B3), r_k is further transformed into the digital domain by ADCs. ADCs are assumed to have the same resolution B as DACs for simplicity. Then based on the AQNM, the quantized version r_k^q of the signal (B3) can be represented by (B4).

$$r_k^q = \alpha^2(\mathbf{w}^k)^H\mathbf{H}_k\mathbf{F}_{\mathrm{RF}}\mathbf{f}_{\mathrm{BB}}^k s_k + \alpha^2(\mathbf{w}^k)^H\mathbf{H}_k\mathbf{F}_{\mathrm{RF}}\sum_{j\neq k}\mathbf{f}_{\mathrm{BB}}^j s_j + \alpha\bar{n}_{q_D,k} + \alpha\bar{n}_k + n_{q_A,k}, \tag{B4}$$

where $\overline{n}_{q_D,k} = (\mathbf{w}^k)^H\mathbf{H}_k\mathbf{F}_{\mathrm{RF}}\mathbf{n}_{q_D}$ with variance $\sigma^2_{\overline{n}_{q_D,k}}$=$(\mathbf{w}^k)^H\mathbf{H}_k\mathbf{F}_{\mathrm{RF}}\mathbf{R}_{\mathbf{n}_{q_D}}{\mathbf{F}_{\mathrm{RF}}}^H{\mathbf{H}_k}^H\mathbf{w}^k$, $\overline{n}_k = (\mathbf{w}^k)^H\mathbf{n}_k$ with variance $\sigma^2_{\overline{n}_k}$=$\left\|\mathbf{w}^k\right\|_F^2\sigma^2$, and n_{q_k} denotes the additive quantization noise with variance $\sigma^2_{n_{q_k}} = \alpha(1-\alpha)(\alpha^2\frac{P}{K}\left\|(\mathbf{w}^k)^H\mathbf{H}_k\mathbf{F}_{\mathrm{RF}}\mathbf{F}_{\mathrm{BB}}\right\|_F^2 + \sigma^2_{\overline{n}_{q_D,k}} + \sigma^2_{\overline{n}_k})$ [12].

Appendix B.2 Channel model

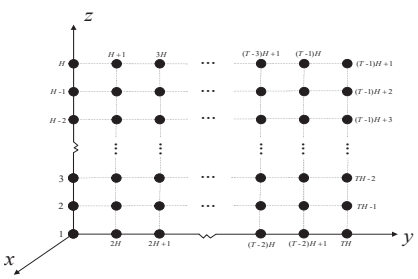

Figure B1 The BS antennas configuration

The mmWave channel will mostly be line-of-sight (LOS), near LOS, or consists of a single reflected path. Therefore, in this work, the mmWave mMIMO channel is modeled by using the clustered Saleh-Valenzuela model [1]. Under this model, channel matrix $\mathbf{H}_k$ is represented as the sum of the contributions from the same N_c scattering clusters, each of which contributes N_{ray} propagation paths to $\mathbf{H}_k$ for $k = 1, 2, \cdots, K$. Therefore, $\mathbf{H}_k$ can be expressed as

$$\mathbf{H}_k{=}\gamma \sum_{i=1}^{N_{\rm c}} \sum_{l=1}^{N_{\rm ray}} g_{i,l}\mathbf{a}_r(\phi_{i,l}^r, \theta_{i,l}^r)\mathbf{a}_t^H(\phi_{i,l}^t, \theta_{i,l}^t), \tag{B5}$$

where $\gamma = \sqrt{\frac{MN}{N_{\rm c}N_{\rm ray}}}$, and $g_{i,l}$ denotes the gain of the lth ray in the ith scattering cluster, $\mathbf{a}_t(\phi_{i,l}^t, \theta_{i,l}^t)$ and $\mathbf{a}_r(\phi_{i,l}^r, \theta_{i,l}^r)$ represent the corresponding transmit array steering vector and the receive array steering vector with the corresponding departure azimuth $\phi_{i,l}^t$, elevation angle $\theta_{i,l}^t$, and the corresponding arrival azimuth $\phi_{i,l}^r$ and arrival elevation angle $\theta_{i,l}^r$, respectively. In fact, $\mathbf{a}_t(\phi_{i,l}^t, \theta_{i,l}^t)$ and $\mathbf{a}_r(\phi_{i,l}^r, \theta_{i,l}^r)$ depend on the transmit and receive array geometry. For the commonly used uniform planar array (UPA) with $M = T \times H$ elements in the yz-plane at the BS, where T and H respectively denote the number of elements in y-axis and z-axis directions, we use the integers $1, 2, \cdots, M$ to respectively label the M BS antennas (shown in Fig. B1), and let $\Xi{=}\{1, 2, \cdots, M\}$. For the adjacent array elements' spacing d being half-wavelength, the corresponding transmit array steering vector is given by formula (B6).

$$\mathbf{a}_t(\phi_{i,l}^t, \theta_{i,l}^t) = \frac{1}{\sqrt{M}}\left[1, \cdots, e^{jkd(t\sin(\phi_{i,l}^t)\sin(\theta_{i,l}^t)+h\cos(\theta_{i,l}^t))}, \cdots, e^{jkd((T-1)\sin(\phi_{i,l}^t)\sin(\theta_{i,l}^t)+(H-1)\cos(\theta_{i,l}^t))}\right], \tag{B6}$$

In (B6), $k = \frac{2\pi}{\lambda}$ with λ denoting the wavelength. Similarly, in the case of a UPA consisting of $T' \times H'$ elements with the adjacent array elements' spacing d in the yz-plane for each user, $\mathbf{a}_r(\phi_{i,l}^r, \theta_{i,l}^r)$ has the similar form as $\mathbf{a}_t(\phi_{i,l}^t, \theta_{i,l}^t)$.

The perfect channel state information of $\mathbf{H}_k$ for $k = 1, 2, \cdots, K$ is assumed to be known to both BS and users in this paper, which can be estimated in practical scenarios.

Appendix C Precoder and combiner optimization design with low-resolution DACs/ADCs

Observing the problem **P1** reveals that maximizing $\sum_{k=1}^{K} R_k$ is sufficient to maximize each R_k in the summation for $k = 1, 2, \cdots, K$, which incurs the following optimization problem with non-convex constraints, given by

$$\begin{aligned}
&\arg \max_{\mathbf{F}_{\rm RF}, \mathbf{F}_{\rm BB}, \mathbf{w}^k} R_k \\
&s.t.\ |\mathbf{F}_{\rm RF}(m,k)| = \begin{cases} \frac{1}{\sqrt{N_{\rm sub}^k}} & if\ \mathbf{F}_{\rm RF}(m,k) \neq 0 \\ 0 & if\ \mathbf{F}_{\rm RF}(m,k) = 0 \end{cases}, \forall\, m, k, \\
&\quad \sum_{k=1}^{K} |\mathbf{F}_{\rm RF}(m,k)| = \frac{1}{\sqrt{N_{\rm sub}^k}}, \forall\, m, \\
&\quad \sum_{m=1}^{M} |\mathbf{F}_{\rm RF}(m,k)|^2 = 1, \forall\, k, \\
&\quad |\mathbf{W}(n,k)| = \frac{1}{\sqrt{N}}, \forall\, n, k, \\
&\quad \|\mathbf{F}_{\rm RF}\mathbf{F}_{\rm BB}\|_F^2 = K.
\end{aligned} \tag{C1}$$

Unfortunately, directly solving the optimization problem (C1) is still hard due to non-convex constraints on optimization parameters $\mathbf{F}$ and $\mathbf{W}$. One observes that maximizing R_k is equivalent to maximizing SINR_k^q for $k = 1, 2, \cdots, K$. However, SINR_k^q has very complicated form and maximizing SINR_k^q involves jointly designing $\mathbf{F}_{\rm RF}$, $\mathbf{F}_{\rm BB}$, and $\mathbf{w}^k$ for $k = 1, 2, \cdots, K$, which not only obtains K different combinations of the analog and the digital precoders, but also leads to a heavy computational burden.

Fortunately, from the formula of SINR_k^q, SINR_k^q is a monotonic function of $\left|(\mathbf{w}^k)^H\mathbf{H}_k\mathbf{F}_{\rm RF}\mathbf{f}_{\rm BB}^k\right|^2$, if the inter-user interference $\sum_{j\neq k}\left|(\mathbf{w}^k)^H\mathbf{H}_k\mathbf{F}_{\rm RF}\mathbf{f}_{\rm BB}^j\right|^2$ is ignored. Inspired by this, maximizing SINR_k^q is split into two stages for DSC-HA with low-resolution DACs/ADCs. First, the design of the analog precoder and combiner is performed to match with the channels of the different users by neglecting the effects of the inter-user interference. Second, after analog precoding and receive combining, a ZF-based digital precoder is designed with the equivalent channel $\overline{\mathbf{H}} = \mathbf{W}^H\mathbf{H}\mathbf{F}_{\rm RF}$ to remove inter-user interference. The details of each stage are now presented.

Appendix C.1 Design analog precoder and receiving combiner

It is seen now that SINR_k^q is a monotonic function of $\left|(\mathbf{w}^k)^H\mathbf{H}_k\mathbf{F}_{\rm RF}\mathbf{f}_{\rm BB}^k\right|^2$, if the inter-user interferences are not taken into consideration. Furthermore, according to the constraint condition $\|\mathbf{F}_{\rm RF}\mathbf{F}_{\rm BB}\|_F^2 = K$, maximizing SINR_k^q is sufficient to maximize $\left\|(\mathbf{w}^k)^H\mathbf{H}_k\mathbf{F}_{\rm RF}\right\|_F$, however, which leads to different analog precoders for different users. It is obviously inconsistent with the actual situation. Hence, in what follows, we decompose the maximization of $\left|(\mathbf{w}^k)^H\mathbf{H}_k\mathbf{F}_{\rm RF}\mathbf{f}_{\rm BB}^k\right|^2$ into a series of subproblems and seek a suboptimal solution with a low complexity.

According the signal model, K users should share the same analog precoder $\mathbf{F}_{\rm RF}$ in the system. In fact, the elements of the kth column of $\mathbf{F}_{\rm RF}$ denote the connection relationship between the kth RF chain associated with the kth user and the M transmit antennas. Based on this and also taking the user fairness into consideration, the analog precoder design in maximizing $\left\|(\mathbf{w}^k)^H\mathbf{H}_k\mathbf{F}_{\rm RF}\right\|_F$ can be relaxed into K separated subproblems by partitioning $\mathbf{F}_{\rm RF}$ into K analog precoding vectors $\mathbf{f}_{\rm RF}^k$ for

$k = 1, 2, \cdots, K$. That is,

$$\begin{aligned} &\arg \max_{\mathbf{w}^k, \mathbf{f}_{\mathrm{RF}}^k} \left| \left(\mathbf{w}^k\right)^H \mathbf{H}_k \mathbf{f}_{\mathrm{RF}}^k \right| \\ &s.t. \left|\mathbf{f}_{\mathrm{RF}}^k(m)\right| = \begin{cases} \frac{1}{\sqrt{N_{\mathrm{sub}}^k}} & if\ \mathbf{f}_{\mathrm{RF}}^k(m) \neq 0 \\ 0 & if\ \mathbf{f}_{\mathrm{RF}}^k(m)=0 \end{cases}, \forall\, m, \\ &\sum_{m=1}^{M} \left|\mathbf{f}_{\mathrm{RF}}^k(m)\right|^2 = 1, \\ &\left|\mathbf{w}^k(n)\right| = \tfrac{1}{\sqrt{N}}, \forall\, n. \end{aligned} \tag{C2}$$

Unfortunately, the separated optimization subproblem in (C2) in terms of $\mathbf{f}_{\mathrm{RF}}^k$ and $\mathbf{w}^k$ cannot be directly solved using the common singular value decomposition because of the special constraints on the elements of $\mathbf{f}_{\mathrm{RF}}^k$. Therefore, we try to solve the optimization subproblem in (C2) alternately by designing $\mathbf{f}_{\mathrm{RF}}^k$ first to make the most of the array gain provided by mMIMO without considering the influence of the analog combining vector $\mathbf{w}^k$, and then solve the analog combining vector $\mathbf{w}^k$ to match the equivalent channel $\mathbf{H}_k \mathbf{f}_{\mathrm{RF}}^k$.

Due to the fact that the elements of $\mathbf{f}_{\mathrm{RF}}^k$ indicate the connection relationships between the M transmit antennas and the kth RF chain associated with the kth user, maximizing $\left|\mathbf{H}_k \mathbf{f}_{\mathrm{RF}}^k\right|$ means a joint implementation of the transmit antennas grouping and analog precoding vector $\mathbf{f}_{\mathrm{RF}}^k$ design under constrained conditions. Thereby, there correspondingly exist K optimization subproblems given in (C3), respectively associated with K optimization subproblems in (C2).

$$\begin{aligned} &\arg \max_{\mathbf{f}_{\mathrm{RF}}^k, A_k} \left|\mathbf{H}_k \mathbf{f}_{\mathrm{RF}}^k\right| \\ &s.t. \left|\mathbf{f}_{\mathrm{RF}}^k(m)\right| = \begin{cases} \frac{1}{\sqrt{N_{\mathrm{sub}}^k}} & if\ \ m \in A_k \\ 0 & if\ \ m \notin A_k \end{cases}, \forall\, m, \\ &\sum_{m=1}^{M} \left|\mathbf{f}_{\mathrm{RF}}^k(m)\right|^2 = 1, \\ &|A_k| = N_{\mathrm{sub}}^k, \end{aligned} \tag{C3}$$

where A_k and $|A_k|$ represent the resultant subset of grouping the transmit antennas associated with kth RF chain and the cardinality of A_k for $k = 1, 2, \cdots, K$, respectively. In fact, K optimization subproblems given in (C3) are interrelated with each other. If $k_1 \neq k_2$ for any k_1, $k_2 \in \{1, 2, \cdots, K\}$, $A_{k_1} \cap A_{k_2} = \emptyset$, and $\sum_{k=1}^{K} |A_k| = M$. However, even if the computational complexity of designing $\mathbf{f}_{\mathrm{RF}}^k$ for $k = 1, 2, \cdots, K$ is not taken into consideration, the optimal transmit antennas grouping of M antennas needs an exhaustive search for $\frac{1}{K!} \sum_{k=0}^{K} (-1)^{K-k} \mathrm{C}_K^k k^M$ combinations [18]. For instance, when $M = 128$ and $K = 8$, this number is 9.7×10^{110}, which is a very gigantic number. Hence, in order to simplify the transmit antennas grouping, we assume M/K is an integer, and each RF chains is connected to the same number of the transmit antennas, i.e., $N_{\mathrm{sub}}^k = |A_k| = M/K$. This assumption to some extent also guarantees the user fairness. Finally, the optimization subproblem in (C3) is simplified as follows.

$$\begin{aligned} &\arg \max_{\mathbf{f}_{\mathrm{RF}}^k, A_k} \left|\mathbf{H}_k \mathbf{f}_{\mathrm{RF}}^k\right| \\ &s.t. \left|\mathbf{f}_{\mathrm{RF}}^k(m)\right| = \begin{cases} \frac{1}{\sqrt{\frac{M}{K}}} & if\ m \in A_k \\ 0 & if\ m \notin A_k \end{cases}, \forall\, m, \\ &|A_k| = \tfrac{M}{K}, \end{aligned} \tag{C4}$$

where $k = 1, 2, \cdots, K$.

To solve the optimization subproblem (C4), an intuitive idea is to select $\frac{M}{K}$ antenna elements from Ξ with the maximum $\|\mathbf{H}_k(:, m)\|_F^2$ to form A_k to be effective, where $\mathbf{H}_k(:, m)$ denotes the mth column of $\mathbf{H}_k$ for $m = 1, 2, \cdots, M$. After that, the elements of $\mathbf{f}_{\mathrm{RF}}^k$ are determined according to the result of the transmit antenna grouping. To this end, the transmit antennas grouping is implemented in an iterative loop among all these K users by taking the user fairness into consideration, and the specific pseudo code is as follows.

$$\begin{aligned} &\Psi = \emptyset \\ &for\ \lambda = 1, 2, \cdots, \tfrac{M}{K} \\ &\quad for\ k = 1, 2, \cdots, K \\ &\quad\quad \overline{m} = \arg \max_{m \in \Xi \setminus \Psi} \{\|\mathbf{H}_k(:, m)\|_F^2\} \\ &\quad\quad A_k = A_k \cup \{\overline{m}\} \\ &\quad\quad \Psi = \Psi \cup \{\overline{m}\} \\ &\quad end \\ &end \end{aligned} \tag{C5}$$

From the transmit antennas grouping strategy above, by trying to maximize $\|\mathbf{H}_k(:, m)\|_F^2$, the set of the transmit antennas Ξ is grouped into K subsets A_k for $k = 1, 2, \cdots, K$ in round robin mode among all K users. Although this transmit antenna grouping strategy is not optimal, it guarantees fairness among users to some degree, but with a relatively low cost of complexity.

With the result of the optimized transmit antennas grouping, it is of interest to point out since $\mathbf{H}_k$ is of $N \times M$-dimension for the user equipped with N antennas, the transmit antennas grouping in (C5) produces N candidate analog precoding vectors $\mathbf{v}_n^k$ to match $\mathbf{H}_k(n, :)$ for $n = 1, 2, \cdots, N$. The mth element in $\mathbf{v}_n^k$ is

$$\mathbf{v}_n^k(m) = \begin{cases} \frac{1}{\sqrt{\frac{M}{K}}} e^{j(-\phi_m^n)} & m \in A_k \\ 0 & m \notin A_k \end{cases}, \tag{C6}$$

where $\phi_m^n = \text{angle}(\mathbf{H}_k(n,m))$ with angle$(\cdot)$ denoting the phase angle operation. After analog precoding with the candidate analog precoding vector $\mathbf{v}_n^k$, the corresponding equivalent channel vector is

$$\mathbf{p}_n^k = \mathbf{H}_k \mathbf{v}_n^k. \tag{C7}$$

Furthermore, based on $\mathbf{p}_n^k$, the zth element of the candidate combining vector $\mathbf{u}_n^k$ is designed to match with the corresponding equivalent channel vector, given by

$$\mathbf{u}_n^k(z) = \frac{1}{\sqrt{N}} e^{j(\varphi_z^n)}, \tag{C8}$$

where $n, z = 1, 2, \cdots, N$ and $\varphi_z^n = \text{angle}\left(\mathbf{p}_n^k(z)\right)$. With $\mathbf{v}_n^k$ and $\mathbf{u}_n^k$, the equivalent channel gain between the kth transmit RF chain of the BS and the kth receive RF chain is

$$\overline{h}_k^n = (\mathbf{u}_n^k)^H \mathbf{H}_k \mathbf{v}_n^k \tag{C9}$$

where $n = 1, 2, \cdots, N$.

With the candidate analog precoding vectors and the candidate combining vectors designed above, in order to maximize the expected equivalent channel gain $\left|\left(\mathbf{w}^k\right)^H \mathbf{H}_k \mathbf{f}_{\text{RF}}^k\right|$, the ultimately optimized analog precoding and combining vectors associated with the kth user should be selected from the candidate analog precoding vectors $\mathbf{v}_n^k$ and the candidate analog combining vector $\mathbf{u}_n^k$ for $n = 1, 2, \cdots, N$. Thereby, the optimized index of $\mathbf{v}_n^k$ and $\mathbf{u}_n^k$ to maximize $\left|\overline{h}_k^n\right|$ is

$$\overline{n} = \arg\max_n \left\{\left|\overline{h}_k^n\right|\right\}. \tag{C10}$$

Based on the result from (C10), the ultimately optimized analog precoding and combining vectors can be expressed as

$$\begin{cases} \mathbf{f}_{\text{RF}}^k = \mathbf{v}_{\overline{n}}^k \\ \mathbf{w}^k = \mathbf{u}_{\overline{n}}^k \end{cases}, \tag{C11}$$

where $k = 1, 2, \cdots, K$. Then the optimized $\mathbf{F}_{\text{RF}}$ and $\mathbf{W}$ are determined.

Appendix C.2 Design the digital precoder

Based on the equivalent channel matrix $\overleftrightarrow{\mathbf{H}} = [\bar{\mathbf{h}}_1^T, \bar{\mathbf{h}}_2^T, \cdots, \bar{\mathbf{h}}_K^T]^T$ after analog precoding and combining, where $\overline{\mathbf{h}}_k = (\mathbf{w}^k)^H \mathbf{H}_k \mathbf{F}_{\text{RF}}$ for $k = 1, 2, \cdots, K$, the digital precoder $\mathbf{F}_{\text{BB}}$ is designed to remove the interference between users according to the ZF criterion. In this sense, the digital precoder $\mathbf{F}_{\text{BB}}$ is

$$\mathbf{F}_{\text{BB}} = \overleftrightarrow{\mathbf{H}}^H (\overleftrightarrow{\mathbf{H}} \overleftrightarrow{\mathbf{H}}^H)^{-1}. \tag{C12}$$

Finally, it should be noted that $\mathbf{F}_{\text{BB}}$ needs to be normalized to meet the power constraint condition to obtain the resultant $\mathbf{F}_{\text{BB}} = \sqrt{K} \frac{\mathbf{F}_{\text{BB}}}{\|\mathbf{F}_{\text{RF}} \mathbf{F}_{\text{BB}}\|_F}$.

By a series of relaxations, the solution for the optimization design of the precoder and combiner for DSC-HA using low-resolution DACs/ADCs is obtained. Although this solution is suboptimal, it makes the optimization problem **P1** tackled. **Algorithm** C1 summarizes the precoder and combiner design for DSC-HA with low-resolution DACs/ADCs. Step 1 initializes the algorithm. Steps 2 to 8 in the table realize dynamically grouping the transmit antennas. The analog precoding and combining vectors associated with the kth user are designed for $k = 1, 2, \cdots, K$ by Steps 9 to 27 according to the resultant subsets of the transmit antennas grouping. The equivalent channel between the transmit and receive RF chains is provided by Steps 28 to 31, and Steps 32 to 33 perform the digital precoder design.

Appendix C.3 Complexity analysis

We analyze the computational complexities of our proposed precoder and combiner for DSC-HA with low-resolution ADCs/DACs, and the comparisons are conducted with the corresponding FC-HA and FSC-HA in this section.

Our proposed precoder and combiner design for DSC-HA with low-resolution DACs/ADCs includes three main components, namely the transmit antennas grouping, the analog precoder and combiner design, and the digital precoder design. The computational complexity required by the transmit antennas grouping is $\mathcal{O}(\frac{M^2}{2} - \frac{M}{K} + \frac{M}{2})$. The analog precoder and combiner design has complexity of $\mathcal{O}(KN(\frac{M}{K} + 2N))$. The design of the digital precoder requires $\mathcal{O}(5K^3)$ computations. Therefore, the computational complexity of our proposed precoder and combiner for DSC-HA with low-resolution DACs/ADCs is $\mathcal{O}(\frac{M^2}{2} + (N - \frac{1}{K} + \frac{1}{2})M + 2KN^2 + 5K^3)$. By carefully analyzing the FC-HA and FSC-HA, the computational complexity of the precoder and combiner design for FC-HA with low-resolution DACs/ADCs requires $\mathcal{O}(KNM + 2KN^2 + 5K^3)$, while the computational complexity for the corresponding FSC-HA is $\mathcal{O}(NM + 2KN^2 + 5K^3)$.

Compared with the precoder and combiner for the corresponding FC-HA, our proposed scheme has a higher complexity when $N \leqslant \frac{M+1-\frac{1}{K}}{2(K-1)}$, but the power consumption and hardware cost for FC-HA is very high. Meanwhile, with the increase of K and/or N, this complexity superiority gradually weakens, even disappears, which will be the truth when more multi-antennas users are simultaneously served by the BS. Additionally, due to the dynamic transmit antennas grouping, the computational complexity for the DSC-HA with low-resolution DACs/ADCs is higher than the design scheme for FSC-HA, but the energy efficiency for DSC-HA improves dramatically, which is confirmed in subsequent Section Appendix E. Hence this additional increase of the computational complexity of our proposed precoder and combiner scheme for DSC-HA with low resolution DACs/ADCs is acceptable.

Algorithm C1 Precoder and combiner design of the precoder and combiner for DSC-HA using low-resolution DACs/ADCs

Input: $\mathbf{H}_k$ for $k = 1, 2, \cdots, K$;
Output: $\mathbf{F}_{\rm RF}$, $\mathbf{F}_{\rm BB}$, $\mathbf{W}$, and A_k for $k = 1, 2, \cdots, K$;
initialize: $\Psi=\emptyset$, $A_k = \emptyset$ for $k = 1, 2, \cdots, K$;
for $i = 1, 2, \cdots, \frac{M}{K}$
  for $k = 1, 2, \cdots, K$
    $\overline{m} = \arg \max\limits_{j \in \Xi \setminus \Psi} \{\|\mathbf{H}_k(:, j)\|_F^2\}$.
    $A_k = A_k \cup \{\overline{m}\}$.
    $\Psi = \Psi \cup \{\overline{m}\}$.
  end for
end for
for $k = 1, 2, \cdots, K$
  for $n = 1, 2, \cdots, N$
    for $m = 1, 2, \cdots, M$
      if $m \in A_k$
        $\mathbf{v}_n^k(m) = \frac{1}{\sqrt{\frac{M}{K}}} e^{-j\text{angle}(\mathbf{H}_k(n,m))}$.
      else
        $\mathbf{v}_n^k(m) = 0$.
      endif
    end for
    $\mathbf{p}_n^k = \mathbf{H}_k \mathbf{v}_n^k$.
    for $z = 1, 2, \cdots, N$
      $\mathbf{u}_n^k(z) = \frac{1}{\sqrt{N}} e^{j\text{angle}\left(\mathbf{p}_n^k(z)\right)}$.
    end for
    $\overline{h}_k^n = (\mathbf{u}_n^k)^H \mathbf{H}_k \mathbf{v}_n^k$.
  end for
  $\overline{n} = \arg \max\limits_{n \in \{1,2,\cdots,N\}} \left\{\left|\overline{h}_k^n\right|\right\}$.
  $\mathbf{f}_{\rm RF}^k = \mathbf{v}_{\overline{n}}^k$.
  $\mathbf{w}^k = \mathbf{u}_{\overline{n}}^k$.
end for
for $k = 1, 2, \cdots, K$
  $\overline{\mathbf{h}}_k = (\mathbf{w}^k)^H \mathbf{H}_k \mathbf{F}_{\rm RF}$
end for
$\overleftrightarrow{\mathbf{H}} = [\overline{\mathbf{h}}_1^T, \overline{\mathbf{h}}_2^T, \cdots, \overline{\mathbf{h}}_K^T]^T$
$\mathbf{F}_{\rm BB} = \overleftrightarrow{\mathbf{H}}^H (\overleftrightarrow{\mathbf{H}} \overleftrightarrow{\mathbf{H}}^H)^{-1}$
$\mathbf{F}_{\rm BB} = \sqrt{K} \frac{\mathbf{F}_{\rm BB}}{\|\mathbf{F}_{\rm RF} \mathbf{F}_{\rm BB}\|_F}$

Appendix D Energy Efficiency Analysis

The system energy efficiency of the proposed precoder and combiner for DSC-HA with low-resolution DACs/ADCs is analyzed in this section. At the same time, the system energy efficiency of the corresponding design schemes for FSC-HA, FC-HA, FD-A, and AP-A is also analyzed for a comparison purpose.

From [12], the system energy efficiency is defined as

$$\chi = \frac{\sum\limits_{k=1}^{K} R_k}{P_{\rm Tot}}, \tag{D1}$$

where the total system power consumption $P_{\rm Tot} = P_{\rm R} + P_{\rm T}$ with $P_{\rm R}$ and $P_{\rm T}$ denoting the power consumption of the user end and BS end, respectively. In the analysis of the power consumption of these different architectures mentioned above, the static power consumption model of the RF front-end is considered, which is also adopted in the works [10], [11], [12], and [14].

To ensure a fair comparison, the analog combiner is adopted at the user end for all related architectures. According to [10], the power consumption at the user end is

$$P_{\rm R} = KP_{\rm LO} + KN(P_{LNA} + P_H + 2P_M) + KNP_{\rm PS} + 2KP_{\rm VGA} + 2KP_{\rm ADC}(B, F_s), \tag{D2}$$

where $P_{\rm LO}$, P_{LNA}, P_H, P_M, $P_{\rm PS}$, $P_{\rm VGA}$, and $P_{\rm ADC}(B, F_s)$ denote the power consumptions of the Local Oscillator (LO) (shared at the single user end), the LNA, the 90^o hybrid and the LO buffer, the mixer, the phase-shifter, the variable gain amplifier (VGA), and the ADC with resolution B and sampling rate F_s, respectively.

For the BS end, the RF front-end of transmitter is composed of two DACs corresponding to I/Q channels, RF chains, PSs (considered only in HA), and PAs. From the direct conversion transceiver architecture, two mixers, two low-pass (LP) filters, a 90^0 hybrid with buffers and a LO shared among all chains together form a single RF chain. The power consumption of a RF chain then is

$$P_{\rm RF} = 2P_{\rm M} + 2P_{\rm LP} + P_{\rm H}, \tag{D3}$$

where $P_{\rm LP}$ is the power consumption of LP filter.

For FSC-HA with low-resolution DACs/ADCs, K RF chains and PAs are employed at the BS end, and a total of M PSs are also used. Thus the power consumption $P_{\rm T}$ at the BS end for FSC-HA with low-resolution DACs/ADCs is given by $P_{\rm T,FSC-HP}$ as

$$P_{\rm T,FSC-HA} = P_{\rm PA} + P_{\rm LO} + K\left(2P_{\rm DAC}(B, f_s) + P_{\rm RF}\right) + MP_{\rm PS}, \tag{D4}$$

where P_{PA} and $P_{\mathrm{DAC}}(B, f_s)$ denote the power consumption of all PAs and a DAC with B resolution bits and sampling at f_s Hz, respectively.

In contrast to FSC-HA with low-resolution DACs/ADCs, a dynamic connection network, which is implemented by a microchip-controlled switch network with the negligible power consumption, is inserted between the RF chains and APSs at the BS side. Therefore, the power consumption P_{T} at the BS end for DSC-HA with low-resolution DACs/ADCs, denoted by $P_{\mathrm{T,FSC-HA}}$, is approximately equal to $P_{\mathrm{T,FSC-HA}}$, given by

$$P_{\mathrm{T,DSC-HA}} \approx P_{\mathrm{T,FSC-HA}}. \tag{D5}$$

For FC-HA with low-resolution DACs/ADCs, the hybrid transmitter employs K RF chains and pairs of DACs, MK PSs, and thus its power consumption P_{T} at the BS end, denoted by $P_{\mathrm{T,FC-HA}}$, is given by

$$P_{\mathrm{T,FC-HA}} = P_{\mathrm{PA}} + P_{\mathrm{LO}} + K\left(2P_{\mathrm{DAC}}(B, f_s) + P_{\mathrm{RF}}\right) + MKP_{\mathrm{PS}}. \tag{D6}$$

For FD-A, M RF chains, pairs of DACs, and PAs are configured at the transmitter, and thus the total power consumption P_{T} at the BS side, denoted by $P_{\mathrm{T,FD-A}}$, is

$$P_{\mathrm{T,FD-A}} = P_{\mathrm{PA}} + P_{\mathrm{LO}} + M\left(2P_{\mathrm{DAC}}(B, f_s) + P_{\mathrm{RF}}\right). \tag{D7}$$

For PA-A, only one RF chain and one pair of DACs are required, and the RF chain connects to M antennas, and then the total power consumption P_{T} at the BS end, denoted by $P_{\mathrm{T,PA-A}}$, is given by

$$P_{\mathrm{T,PA-A}} = P_{\mathrm{PA}} + P_{\mathrm{LO}} + 2P_{\mathrm{DAC}}(B, f_s) + P_{\mathrm{RF}} + MP_{\mathrm{PS}}. \tag{D8}$$

The specific values of these components in formulas (D2) to (D8) can be found in [10] and [14].

Appendix E Numerical Results

Because of the difficulty of theoretical analysis of the effects of the resolution of DACs/ADCs, SNR and other factors on system performance, the numerical results are provided in this section to evaluate the performance of the proposed precoder and combiner for DSC-HA with low-resolution DACs/ADCs. In the numerical simulation, channel parameters are given by $N_c = 2$ cluster with $N_{ray} = 10$ rays per cluster for all users due to the sparsity of the mmWave channels. All clusters are of unit power. The azimuth and elevation angles of arrival and departure all obey the Laplacian distribution. For simplicity of exposition, the mean angles of them are uniformly distributed in $[0, 2\pi]$ and the angular spread are set as $\frac{\pi}{18}$ in the azimuth and elevation domain. $K = 8$ and $d = \frac{\lambda}{2}$. In the paper, the SNR is defined as $\frac{P}{K\sigma^2}$.

Appendix E.1 System Sum Rate versus SNR

For $M = T \times H = 8 \times 16$ and $N = T' \times H' = 2 \times 4$, the system sum rates of our proposed precoder and combiner for DSC-HA versus SNR for $B = 1$ and $B = 3$ is shown in Fig. E1 and Fig. E2, respectively, and the comparisons are conducted over several schemes for different architectures. From these figures, the system sum rates of these precoder and combiner design schemes for different architectures improve with the increase of the SNR. Since the precoder scheme for FD-A has the ability to control both the amplitude and phase of the transmitted signal, the system sum rate for FD-A is significantly higher than that for FC-HA in the low SNR range. However, as the SNR increases, due to the large analog beamforming gain provided by the FC-HA, the superiority of FD-A over FC-HA disappears gradually. Meanwhile, because FC-HA can provide significantly higher array gain than SC-HA, the performance gap between DSC-HA and FC-HA is still obvious, but the power consumption and hardware cost of the latter are much higher than that of FSC-HA. For DSC-HA with low-resolution DACs/ADCs, the purpose of designing the analog precoding and combining vectors is to match different users' channel to fully utilize the array gain provided by mMIMO. Therefore, the system sum rate for DSC-HA is superior to that for FSC-HA. Additionally, due to the single RF chain required by PA-A, its achievable sum rate is the smallest.

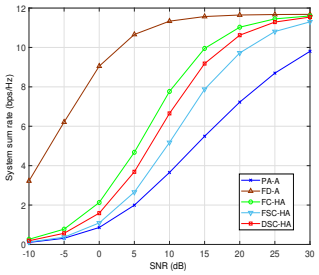

Figure E1 System sum rate versus SNR with $B = 1$ (bit)

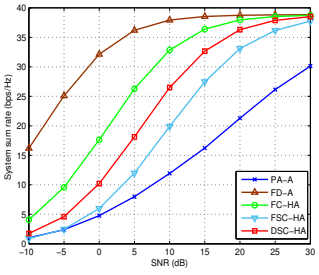

Figure E2 System sum rate versus SNR with $B = 3$ (bit)

Appendix E.2 System Sum Rate versus DACs/ADCs Resolution

Fig. E3 and Fig. E4 show the system sum rates versus DACs/ADCs resolution B with $M = T \times H = 8 \times 16$ and $N = T' \times H' = 2 \times 4$ for SNR = -5 (dB) and 10 (dB), respectively. From these two figures, the system sum rates of the precoder and combiner design schemes for different architectures improve with the increase of the resolution of the ADCs B. However, when $B > 4$, the system sum rates of these schemes tend to be stable. Hence it can be concluded that optimal DACs/ADCs resolution B is 4 (bits) for these precoder and combiner design schemes for different architectures, including our proposed precoder and combiner for DSC-HA. The similar conclusion can be reached for different SNRs and/or antenna configurations. Thereby, in the following experiments, we set $B = 4$.

Additionally, from E3 and Fig. E4, for low SNR (i.e. SNR=-5 (dB)), the PA-A seems to have a better performance than the FSC-HA. This is because for low SNR, the influence of background noise on system performance is dominant compared with that of inter-user interference, while PA-A has only one RF chain, which can use all BS antennas to obtain stronger beamforming gain to weaken the influence of noise. For FSC-HA, each RF is connected to the fixed disjoint subset of the total transmit antennas to design hybrid precoding for different users, which can only obtain relatively weak beamforming gain for different users, Therefore, the ability of suppressing strong background noise is weak. With the increase of SNR, the influence of inter-user interference on system performance becomes dominant. FSC-HA can effectively eliminate inter-user interference by designing hybrid precoder, while PA-A can't do anything about it. Therefore, FSC-HA has better performance than PA-A for high SNR (i.e. SNR=10 (dB)).

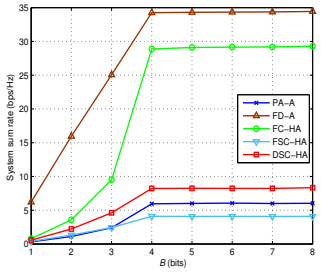

Figure E3 System sum rate versus B for different architectures with SNR=-5 (dB)

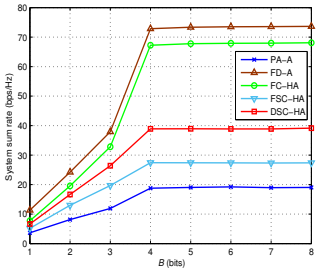

Figure E4 System sum rate versus B for different architectures with SNR=10 (dB)

Appendix E.3 System Sum Rate versus Number of BS Antennas $M = T \times H$

Fig. E5 and Fig. E6 provide the system sum rates versus $M = T \times H$ of several precoder and combiner design schemes for different architectures with $N = T' \times H' = 2 \times 4$ for SNR = -5 (dB) and 10 (dB), respectively. Due to the improved array gain with the increase of M, the system sum rates of all schemes improve significantly, except the precoder and combiner design scheme for PA-A. For high SNR case in Fig. E6, our proposed precoder and combiner for DSC-HA with low resolution DACs/ADCs obviously outperforms the precoder and combiner design schemes for FSC-HA and PA-A. Although the obvious performance gap between FD-A and DSC-HA with the optimally designed precoder and combiner is observed, the complexity of the required hardware circuits of DSC-HA, as a special case of SC-HA, is significantly reduced, which means DSC-HA can achieve a relatively good tradeoff between the hardware cost and performance.

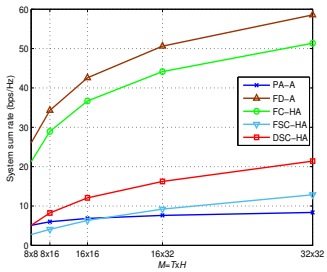

Figure E5 System sum rate versus M for different architecture with SNR=-5 (dB)

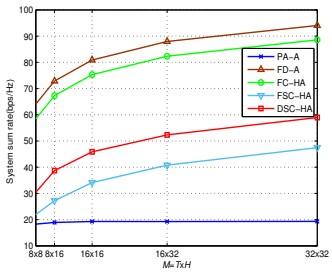

Figure E6 System sum rate versus M for different architecture with SNR=10 (dB)

Appendix E.4 System Energy Efficiency versus DACs/ADCs Resolution B

Fig. E7 and Fig. E8 show the system energy efficiency versus the DACs/ADCs resolution B of several precoder and combiner design schemes for $M = T \times H = 8 \times 16$ and $N = T' \times H' = 2 \times 4$ with SNR=-5 (dB) and 10 (dB), respectively. It can be concluded from the figures, for the DACs/ADCs with resolution $B = 4$, the maximum system energy efficiency achieves for almost all precoder and combiner design schemes. Moreover, for the low SNR (i.e., SNR = -5 (dB)), the precoder and combiner design scheme for FC-HA has the highest energy efficiency because the power consumption of the FC-HA is dramatically lower than that of FD-A, but the gap of the system sum rate between the FC-HA and FD-A is relatively small. Meanwhile, the precoder and combiner design scheme for PA-A has a superiority in terms of energy efficiency on the precoder and combiner design schemes for FD-A, FSC-HA and DSC-HA due to its obvious low power consumption for low SNR. For the high SNR (i.e., SNR=10 (dB)), our proposed precoder and combiner for DSC-HA achieves the best system energy efficiency when $B \leqslant 3$, and for $B = 4$ even though its energy efficiency is worse than the precoder and combiner design scheme for FC-HA, the hardware cost and power consumption of FC-HA are obviously higher than DSC-HA.

Furthermore, the energy efficiency of the precoder and combiner design scheme for FC-HA with the optimal resolution $B = 4$ is obviously better than that for DSC-HA owing much to the obvious superiority over the system sum rate of DSC-HA, but the hardware cost of the former is much higher than the latter.

Additionally, the number of the power-hungry RF chains and DACs required in FD-A is far greater than in HA, which leads to somehow a lower energy efficiency for FD-A than for HA, including DSC-HA and FSC-HA at high SNR (although the FD-A had slight energy efficiency advantage over HA at low SNR for ADCs/DACs resolution $B \leqslant 3$ due to the obvious system sum rate superiority of FD-A over HA).

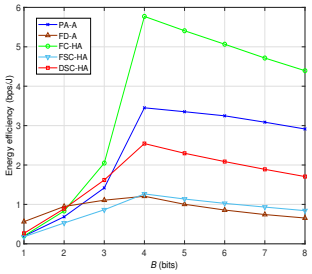

Figure E7 Energy efficiency versus ADCs/DACs resolution B with SNR=-5 (dB)

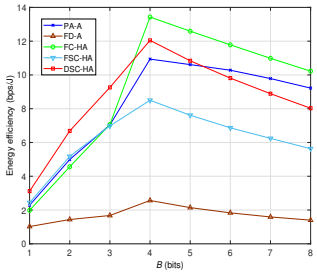

Figure E8 Energy efficiency versus ADCs/DACs resolution B with SNR=10 (dB)

Appendix E.5 System Energy Efficiency versus System Sum Rate

Fig. E9 and Fig. E10 show the trade-off of the system energy efficiency versus system sum rate with $M = T \times H = 8 \times 16$ and $N = T' \times H' = 2 \times 4$ for SNR=-5 (dB) and 10 (dB), respectively. There exist 8 points on each curve associated to one specific precoding scheme, which are respectively related to DACs/ADCs with resolution $B = 1, 2, \ldots, 8$. From these two figures, we observe that as B is increased, the curves first reach upward and right to the highest, and then drop. The highest point just corresponds to the combination of the system energy efficiency and system sum rate for $B = 4$, namely, the system energy efficiency of all precoding and combining schemes declines when DACs/ADCs resolution $B > 4$, which coincides with the simulation results in Fig. E7 and Fig. E8. Under the low SNR, the superiority of the precoder and combiner for FC-A is very obvious. However, our proposed precoder and combiner for DSC-HA achieves obvious advantage compared to the precoder and combiner design schemes for FD-A, FSC-HA, and PA-A for high SNR. Although its performance is poorer than the precoder and combiner design scheme for FC-HA, the latter requires much higher hardware cost and power consumption than DSC-HA.

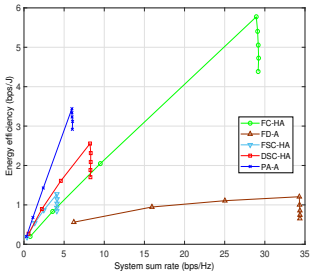

Figure E9 Energy efficiency versus system sum rate with SNR=-5 (dB)

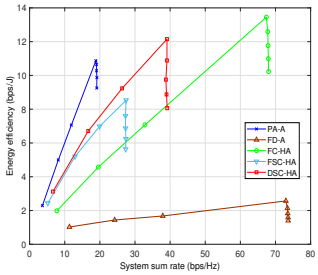

Figure E10 Energy efficiency versus system sum rate with SNR=10 (dB)

Appendix E.6 Transmit Antenna Grouping Results for DSC-HA with low-resolution DACs/ADCs

For two random channel utilizations with $M = T \times H = 8 \times 16$ and $N = T' \times H' = 2 \times 4$, Table E1 provides the transmit antenna grouping results for DSC-HA with low-resolution DACs/ADCs. As can be seen from Table E1, it is concluded that the transmit antennas are dynamically grouped so as to be matched with the different user's channel in the DSC-HA. Based on this, the analog precoding vectors and the combining vector are designed. For this reason, our proposed precoder and combiner for DSC-HA with low-resolution DACs/ADCs has much higher system sum rate than that for the corresponding FSC-HA.

Table E1 The transmit antennas grouping results for two random channel utilizations

	A_1	A_2	A_3	A_4	A_5	A_6	A_7	A_8
1	{7, 36, 50, 73, 74, 75, 76, 77, 104, 105, 106, 112, 113, 115, 116, 122}	{4, 5, 6, 28, 46, 47, 48, 63, 67, 78, 95, 96, 97, 98, 99, 108}	{22, 24, 25, 26, 27, 29, 30, 31, 32, 33, 37, 40, 43, 44, 45, 66}	{8, 9, 12, 13, 49, 62, 65, 66, 86, 89, 90, 107, 110, 111, 114, 117}	{57, 58, 60, 61, 68, 69, 70, 71, 72, 100, 101, 118, 119, 121, 127, 128}	{1, 11, 14, 15, 16, 17, 19, 20, 21, 22, 52, 64, 92, 93, 94, 126}	{10, 34, 35, 51, 56, 59, 82, 83, 84, 85, 87, 88, 120, 123, 124, 125}	{2, 3, 18, 38, 39, 41, 42, 53, 54, 55, 79, 80, 81, 102, 103, 109}
2	{1, 2, 3, 4, 6, 12, 92, 110, 117, 118, 119, 120, 121, 122, 123, 128}	{18, 46, 48, 54, 55, 60, 66, 67, 68, 69, 71, 77, 79, 90, 97, 98}	{5, 8, 9, 29, 30, 31, 32, 52, 56, 57, 58, 104, 108, 124, 125, 126}	{10, 11, 14, 15, 16, 17, 25, 26, 27, 28, 33, 62, 63, 81, 106, 107}	{19, 20, 58, 80, 82, 83, 84, 85, 86, 87, 88, 112, 113, 114, 115, 127}	{21, 22, 39, 42, 59, 61, 64, 65, 70, 72, 73, 75, 94, 95, 96, 109}	{23, 24, 35, 37, 38, 40, 41, 44, 50, 53, 89, 99, 100, 101, 102, 103}	{7, 13, 34, 36, 43, 45, 47, 49, 51, 74, 76, 91, 93, 105, 111, 116}

References

1 Ayach O E, Rajagopal S, Abu-Surra S, et al. Spatially sparse precoding in millimeter wave MIMO systems. IEEE Trans Wireless Commun, 2014, 13: 1499-1513

2 Wang Z, Li M, Liu Q, et al. Hybrid precoder and combiner design with low-resolution phase shifters in mmWave MIMO systems. IEEE J Sel Topics Signal Process, 2018, 12: 256-269
3 Li J, Xiao L, Xu X, et al. Energy-efficient Butler-matrix-based hybrid beamforming for multiuser mmWave MIMO system. Sci China Info Sci, 2017, 60: 080304
4 Chen C, Dong Y, Cheng X, et al. Low-resolution PSs based hybrid precoding for multiuser communication systems. IEEE Trans Veh Technol, 2018, 67: 6037-6047
5 Zhu X, Wang Z, Dai L, et al. Adaptive hybrid precoding for multiuser massive MIMO. IEEE Commun Lett, 2016, 20: 776-779
6 Han S, I C-L, Xu Z, et al. Large-scale antenna systems with hybrid analog and digital beamforming for millimeter wave 5G. IEEE Commun Mag, 2015, 53: 186-194
7 Jing X, Li L, Liu H, et al. Dynamically-connected hybrid precoding scheme for millimeter wave massive MIMO systems. IEEE Commun Lett, 2018, 22: 2583-2586
8 Walden R H. Analog-to-digital converter survey and analysis. IEEE J Sel Areas Commun, 1999, 17: 539-550
9 Zhang J, Dai L, Li X, et al. On low-resolution ADCs in practical 5G millimeter-wave massive MIMO systems. IEEE Commun Mag, 2018, 56: 205-211
10 Roth K, Nossek J A. Achievable rate and energy efficiency of hybrid and digital beamforming receivers with low resolution ADC. IEEE J Sel Areas Commun, 2017, 35: 2056-2068
11 Mo J, Alkhateeb A, Abu-Surra S, et al. Hybrid architectures with few-bit ADC receivers: achievable rates and energy-rate tradeoffs. IEEE Trans Wireless Commun, 2017, 16: 2274-2287
12 Abbas W B, Gomez-Cuba F, Zorzi M. Millimeter wave receiver efficiency: a comprehensive comparison of beamforming schemes with low resolution ADCs. IEEE Trans Wireless Commun, 2017, 16: 8131-8146
13 Choi J, Lee G, Evans B L. Two-stage analog combining in hybrid beamforming systems with low-resolution ADCs. IEEE Trans Signal Process, 2019, 67: 2410-2425
14 Ribeiro L N, Schwarz S, Rupp M, et al. Energy efficiency of mmWave massive MIMO precoding with low-resolution DACs. IEEE J Sel Topics Signal Process, 2018, 12: 298-3124
15 Vlachos E, Kaushik A, Thompson J, Energy efficient transmitter with low resolution DACs for massive MIMO with partially connected hybrid architecture. In: Proceedings of IEEE Vehicular Technology Conference (VTC Spring), Porto, 2018
16 Zhang J, Dai L, Sun S. On the spectral efficiency of massive MIMO systems with low-resolution ADCs. IEEE Commun Lett, 2016, 20: 842-845.
17 Fan L, Jin S, Wen C-K, et al. Uplink achievable rate for massive MIMO systems with low-resolution ADC. IEEE Commun Lett, 2015, 19: 2186-2189
18 Park S, Alkhateeb A, Heath R W. Dynamic subarrays for hybrid precoding in wideband mmWave MIMO systems. IEEE Trans Wireless Commun, 2017, 16: 2907-2920